Thin or bulky: Optimal aspect ratios for ship hulls

Jean-Philippe Boucher, Romain Labbé, Christophe Clanet, and Michael Benzaquen*
LadHyX, UMR 7646 du CNRS, École polytechnique, 91128 Palaiseau Cedex, France

(Received 28 March 2018; published 30 July 2018)

Empirical data reveal a broad variety of hull shapes among the different ship categories. We present a minimal theoretical approach to address the problem of ship hull optimization. We show that optimal hull aspect ratios result—at given load and propulsive power—from a subtle balance among wave drag, pressure drag, and skin friction. Slender hulls are more favorable in terms of wave drag and pressure drag, while bulky hulls have a smaller wetted surface for a given immersed volume, thus reducing skin friction. We compare our theoretical results to real data and discuss discrepancies in the light of hull designer constraints, such as stability and maneuvrability.

DOI: 10.1103/PhysRevFluids.3.074802

I. INTRODUCTION

The long-standing subject of ship hull design is without a doubt one of infinite complexity. Constraints may significantly vary from one ship class to another. When designing a sailing boat [see Fig. 1(a)], stability and maneuvrability are of paramount importance [1–4]. Liners and warships must be able to carry a maximal charge and resist rough sea conditions. Ferries and cruising ships [see Fig. 1(b)] must be sea-kindly such that passengers do not get seasick. However, all ship hulls share one crucial constraint: They must suffer the weakest drag possible in order to minimize the required energy to propel themselves, or similarly maximize their velocity for a given propulsive power. Of particular interest is the case of rowing boats [see Fig. 1(c)] [5,6], sprint canoes, and sprint kayaks as they do not really have other constraints than the latter. Indeed, maneuvrability is not relevant as they only have to go along straight lines, stability is at its edge, and they only need to carry the athletes, usually on very calm waters.

In Fig. 2, the length-to-width aspect ratio (ℓ/w) of different kinds of bodies moving at the water surface is plotted against their Froude number (see Table I for details). The Froude number is defined as $\mathrm{Fr} = U/\sqrt{g\ell}$ with U being the hull velocity, g being the acceleration of gravity, and ℓ being the length of the hull [see Fig. 1(c)]. As one can see, different ship categories tend to gather into clusters. These groups display very different aspect ratios, from 2–3 to about 30, even in the same Froude number regime. The highest aspect ratios are reached for rowing boats ($\ell/w \approx 30$, $\mathrm{Fr} \approx 0.5$). The majority of ships stand on the left-hand side of the plot ($\mathrm{Fr} \lesssim 0.7$). For $\mathrm{Fr} \gtrsim 0.7$, most hulls can no longer be considered as *displacement* hulls (weight balanced by buoyancy) but rather as *planing* hulls (weight balanced by hydrodynamic lift) and thus have a much smaller immersed volume [4]. Here we wonder how all these shapes compare to the optimal aspect ratios in terms of drag.

For a fully immersed body moving at large Reynolds numbers, the drag (also called *profile drag*) is the sum of two contributions [2,4,7]: (i) the skin-friction drag, which comes from the frictional forces exerted by the fluid along the surface of the body (dominant for a streamlined body, such as a plate parallel to the flow) and (ii) the pressure drag, which results from the separation of the flow and the creation of vortices (dominant for a bluff body such as a sphere) [7]. One additional

*Corresponding author: michael.benzaquen@polytechnique.edu

FIG. 1. Pictures of (a) a 44-ft sailing boat: length-to-width aspect ratio 3 and typical Froude number 0.6, (b) the *Queen Mary 2* liner: length-to-width aspect ratio 8.4 and typical Froude number 0.26, and (c) a coxless quadruple scull rowing boat: length-to-width aspect ratio 31 and typical Froude number 0.54. See Table I for details and characteristics of other boats.

force arises when moving at the air-water interface: the *wave resistance* or *wave drag* [8–10]. This force results from the generation of surface waves which continuously remove energy to infinity. It is interesting to notice that many animals have air or water as a natural habitat but only a few (e.g., ducks, muskrats, and sea otters) actually spend most of their time at the water surface [11,12].

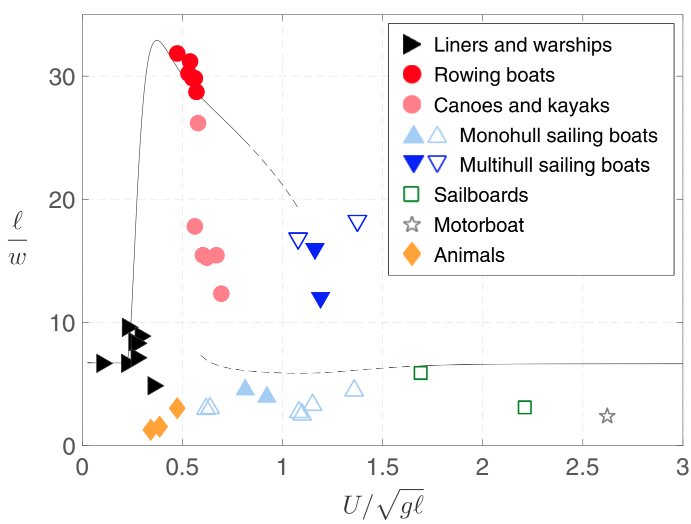

FIG. 2. Length-to-width aspect ratio ℓ/w as a function of Froude number $U/\sqrt{g\ell}$ for different kinds of bodies moving at the water surface (see Table I for details). Solid symbols represent displacement hulls, whereas open symbols indicate planing hulls. The aspect ratio for multihulls is computed for each hull independently. The black line corresponds to the optimal aspect ratio; see Sec. III. Solid lines indicate global optima, while dashed lines signify local optima.

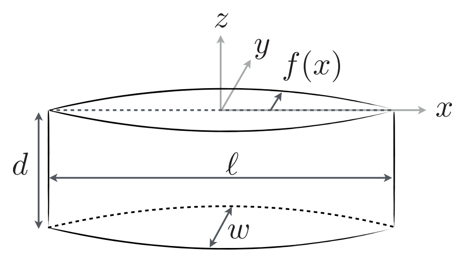

FIG. 3. Schematics of the simplified hull geometry considered in this study. The hull of length ℓ, width w, and draft d has a constant horizontal cross section, which is defined by $y = f(x)\mathbb{1}_{z\in[-d,0]}$. Note that only the part of the hull immersed in the water is represented.

As one can expect, a number of technological advances have been developed over the years, such as bulbous bows intended to reduce wave drag through destructive interference [3,13,14]. There exists an extended literature of numerical and experimental studies dedicated to the optimization of ship hulls. Quite surprisingly, some of them only consider wave drag in the optimisation setup (see, e.g., Refs. [15–17]). Others consider both the skin drag and the wave drag [14,18,19]. Very few consider the pressure drag [20], as most studies address slender streamlined bodies for which the boundary layer does not separate, leading to a negligible pressure drag. The complexity of addressing analytically this optimization problem comes from the infiniteness of the search space. Indeed, without any geometrical constraints, the functions defining the hull geometry can be anything, and computing the corresponding drag can become an impossible task.

Here we present a minimal approach to address the question of optimal hull aspect ratios in the presence of skin drag, pressure drag, and wave drag. Let us stress that we do not claim that our results are quantitative but rather present qualitative ideas and general trends on the very complex matter of ship hull optimization. We first consider a model hull shape with a minimum number of parameters and derive the expression of the total drag coefficient. Then we perform the shape optimization at given propulsive power and load. Finally we compare our results to the empirical data and discuss concordances and discrepancies.

II. WAVE AND PROFILE DRAG

In order to account in a minimal way for the wide variety of hull shapes, we restrict the discussion to two-dimensional hulls (namely hulls with a constant horizontal cross section; see Fig. 3). Following the generic parametrization of hull shapes with respect to the central plane [8,21–23], we let $y = f(x)\mathbb{1}_{z\in[-d,0]}$ be the compact support hull boundary. We define the length ℓ, width w, and draft d and introduce the dimensionless coordinates through $x = \tilde{x}\ell$, $y = \tilde{y}\ell$, and $z = \tilde{z}\ell$ as well as $f(x) = \tilde{f}(\tilde{x})w$ [24]. We further define the aspect ratios $\alpha = \ell/w$ and $\beta = \ell/d$.

There exist two main theoretical models to estimate the wave resistance, both assuming that the fluid is incompressible, inviscid, irrotational, and infinitely deep. Havelock suggested replacing the moving body by a moving pressure disturbance [9,10]. This first model allows us to compute the far-field wave pattern as well as the wave resistance [17,25,26] but it is too simple to account for the exact shape of the hull and especially to study the effect of the draft. The second model was developed by Michell for slender bodies [8,21,27]: The linearized potential flow problem with a distribution of sources on the center plane of the hull is solved to get the expression of the wave resistance. The advantage of the latter is that it gives a very practical formula in the sense that it only takes as inputs the parametric shape of the hull and its velocity, with no need of inferring the corresponding pressure distribution. Using Michell's approach, we compute the wave drag $R_\mathrm{w} = \rho\Omega^{2/3}U^2C_\mathrm{w}$ where ρ is the water density and $\Omega = \ell w d$ [28]. The wave drag coefficient

C_w writes (see Appendix A)

$$C_\mathrm{w}(\mathrm{Fr},\alpha,\beta) = \frac{4\beta^{2/3}}{\pi\alpha^{4/3}\mathrm{Fr}^4}\, G_{\tilde{f}}(\mathrm{Fr},\beta)\ , \tag{1}$$

where we have defined:

$$G_{\tilde{f}}(\mathrm{Fr},\beta) = \int_1^{+\infty} \frac{|I_{\tilde{f}}(\lambda,\mathrm{Fr},\beta)|^2}{\sqrt{\lambda^2-1}}\,\mathrm{d}\lambda$$

$$I_{\tilde{f}}(\lambda,\mathrm{Fr},\beta) = (1-e^{-\lambda^2/(\beta\mathrm{Fr}^2)}) \int_{-\frac{1}{2}}^{\frac{1}{2}} \tilde{f}(\tilde{x})e^{i\lambda\tilde{x}/\mathrm{Fr}^2}\,\mathrm{d}\tilde{x}\ . \tag{2}$$

To compute the wave-drag we consider a Gaussian hull profile:

$$\tilde{f}(\tilde{x}) = \tfrac{1}{2}\exp[-(4\tilde{x})^2]\ . \tag{3}$$

This particular kind of profile allows to analytically compute the wave resistance coefficient. The choice of this profile in comparison with more realistic profiles has no qualitative impact on our main results (see Appendix A).

The profile drag R_p is the sum of the skin drag R_s which scales with the wetted surface and the pressure drag (or form drag) R_f which scales with the main cross section. Given the typical Reynolds numbers for ships (ranging from 10^7 to 10^9), both the skin and pressure contributions scale with U^2 and the profile drag can be written as $R_\mathrm{p} = R_\mathrm{s} + R_\mathrm{f} = \rho\Omega^{2/3}U^2C_\mathrm{p}$ with (see Appendix B)

$$C_\mathrm{p}(\alpha,\beta) = \frac{C_\mathrm{d}(\alpha)\beta^{2/3}}{\alpha^{1/3}}\left[a_{\tilde{f}} + \frac{\alpha}{\beta}b_{\tilde{f}}(\alpha)\right], \tag{4}$$

where $C_\mathrm{d}(\alpha)$ is the profile drag coefficient of the hull, and where

$$a_{\tilde{f}} = \int_{-\frac{1}{2}}^{\frac{1}{2}} \tilde{f}(\tilde{x})\,d\tilde{x}, \tag{5a}$$

$$b_{\tilde{f}}(\alpha) = \int_{-\frac{1}{2}}^{\frac{1}{2}} [1+\tilde{f}'(\tilde{x})^2/\alpha^2]^{1/2}\,d\tilde{x}\ . \tag{5b}$$

The evolution of the profile drag coefficient C_d with α was empirically derived for streamlined bodies [7]: $C_\mathrm{d}(\alpha) = C_\mathrm{f}(1+2/\alpha+60/\alpha^4)$ with C_f being the skin drag coefficient for a plate. The term $(1+2/\alpha)$ refers to the skin friction, while the term $60/\alpha^4$ corresponds to the pressure drag [29]. In the considered regimes, the skin drag coefficient is only weakly dependent on the Reynolds number [7] (see Appendix B). We thus consider here a constant skin drag coefficient $C_\mathrm{f} = 0.002$, corresponding to a Reynolds number $\mathrm{Re} \simeq 10^8$.

The total drag force on the hull reads $R = R_\mathrm{w} + R_\mathrm{p} = \rho\Omega^{2/3}U^2C$, where $C(\alpha,\beta,\mathrm{Fr}) =$

$$\frac{\beta^{2/3}}{\alpha^{4/3}}\left\{\frac{4}{\pi\mathrm{Fr}^4}G_{\tilde{f}}(\mathrm{Fr},\beta) + C_\mathrm{d}(\alpha)\alpha\left[a_{\tilde{f}} + \frac{\alpha}{\beta}b_{\tilde{f}}(\alpha)\right]\right\}. \tag{6}$$

Within the present framework and choice of dimensionless parameters, the total drag coefficient is thus completely determined by the three dimensionless variables α, β, and Fr, together with the function $\tilde{f}$. Let us stress that this expression of the total drag coefficient is only expected to be accurate for slender hulls, as required in Michell's model [21,27,30].

III. OPTIMAL HULLS

We now seek the optimal hull shapes, that is, the choice of parameters that minimizes the total drag for a given load (equivalently immersed volume through the Archimedes principle) and given propulsive power, consistent with operational conditions. Before engaging in any calculations, let

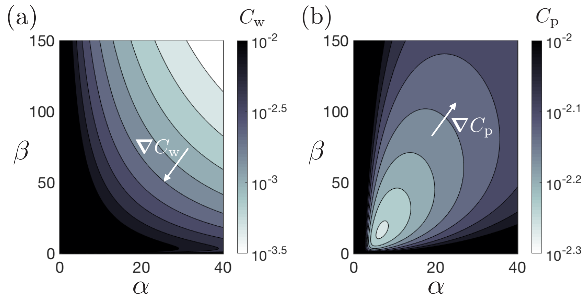

FIG. 4. Contour plots of (a) the wave drag coefficient C_w and (b) the profile drag coefficient C_p as a function of the aspect ratios α and β. For the wave drag coefficient, we set $\mathrm{Fr} = 0.5$. In both plots, black regions correspond to $C_{p/w} \geqslant 10^{-2}$ and arrows indicate the direction of the gradient.

us stress that the optimal aspect ratios will naturally result from a subtle balance among skin drag, pressure drag, and wave drag. Indeed, on the one hand, reducing skin drag amounts to minimizing the wetted surface which corresponds to rather bulky hulls [31], while, on the other hand, reducing wave drag or pressure drag pushes towards rather slender hulls. Figure 4 displays the contour plots of C_p and C_w as function of (α,β) [32]. One notices that for sufficiently large α and β the gradients ∇C_p and ∇C_w roughly point in opposite directions.

To close the problem, we define the imposed propulsive power $\mathcal{P} = RU$. Using $U = \mathrm{Fr}[\alpha\beta\Omega g^3]^{1/6}$, one obtains

$$\mathrm{Fr}^3\sqrt{\alpha\beta}\,C(\alpha,\beta,\mathrm{Fr}) = \Pi\ , \tag{7}$$

where $C(\alpha,\beta,\mathrm{Fr})$ is given by Eq. (6), and where we have defined the rescaled and dimensionless power:

$$\Pi = \frac{\mathcal{P}}{\rho g^{3/2}\Omega^{7/6}}\ . \tag{8}$$

Minimizing the total drag coefficient C as given by Eq. (6) with respect to α, β, and Fr, under the constraint given by setting the dimensionless power Π in Eq. (7), yields the optimal set of parameters ($\alpha^\star$, $\beta^\star$, $\mathrm{Fr}^\star$) for the optimal hull geometry at given load (equivalently Ω) and given propulsive power $\mathcal{P}$.

This optimization is performed numerically using an interior-point algorithm [33,34]. The optimal parameters and the resulting total drag coefficient $C^\star = C(\alpha^\star,\beta^\star,\mathrm{Fr}^\star)$ as function of dimensionless power Π are presented in Fig. 5, together with the empirical data points for comparison. Interestingly, the optimization yields two separate solutions (see orange and green branches) corresponding to two local optima. For $\Pi \leqslant \Pi_c$ (resp. $\Pi \geqslant \Pi_c$) with $\Pi_c \approx 0.2$, the orange (resp. green) branch constitutes the global optimum, consistent with a lower total drag coefficient $C^\star$ [see Fig. 5(d)]. As one can see in Figs. 5(a) and 5(b), the optimal aspect ratios $\alpha^\star$ and $\beta^\star$ show very similar evolutions with Π. On the one hand, both of them are maximal around $\Pi_{max} \approx 0.03$ corresponding to $\mathrm{Fr}_{max} \approx 0.4$, that is the maximum wave drag regime (see Fig. 6 in Appendix A). This is consistent with the idea that thin and shallow hulls are favorable in terms of wave drag, as illustrated in Fig. 4(a). On the other hand, for $\Pi \ll \Pi_{max}$ or $\Pi \gg \Pi_{max}$ the wave drag becomes negligible compared to the profile drag, and one recovers the optimal aspect ratios in the absence of wave drag: $\alpha^\star \simeq 7$ and $\beta^\star \simeq 10$. Figure 5(c) shows that the optimal Froude number $\mathrm{Fr}^\star$ increases with Π. Like for $\alpha^\star$ and $\beta^\star$, there is a shift of value from $\mathrm{Fr}^\star \approx 0.8$ to $\mathrm{Fr}^\star \approx 1.7$, for $\Pi = \Pi_c$, which indicates that in this setting $0.8 < \mathrm{Fr} < 1.7$ is never a suitable choice. This shift is also made visible in Fig. 2, where the optimal aspect ratio $\alpha^\star$ is plotted against the Froude number. These results obviously depend on the Reynolds number but only weakly. Let us stress that while for the optimal geometries ($\alpha^\star$, $\beta^\star$) the profile drag is always

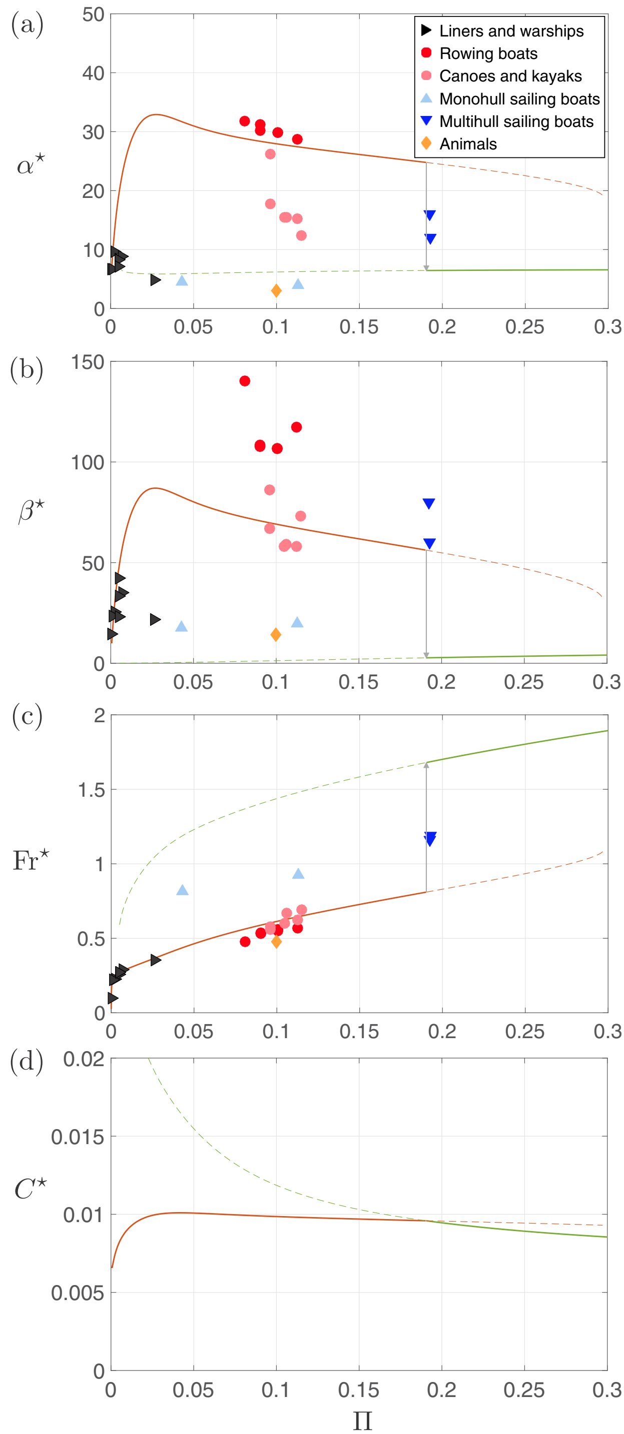

FIG. 5. (a) Optimal aspect ratio $\alpha^\star$, (b) optimal aspect ratio $\beta^\star$, (c) optimal Froude number $\mathrm{Fr}^\star$, and (d) corresponding value of the total drag coefficient $C^\star = C(\alpha^\star,\beta^\star,\mathrm{Fr}^\star)$, as a function of the dimensionless power Π. The curves in orange and green represent the two optimal branches. Solid and dashed lines indicate global and local optima, respectively.

the dominant force regardless of the Froude number, our study shows that it is crucial to consider the wave drag in the optimization.

IV. DISCUSSION

Our work provides a self-consistent framework to understand and discuss the design of existing boats. Figure 5 confronts the real data with the calculated optimal geometries. As one can see, while some ship categories are found to be in good agreement with the theoretical predictions (such as liners and warships), others are very far from the computed optima (such as monohull sailing boats). Discrepancies with empirical data might primarily come from other constraints on the design of the boat which can prevail on the minimization of the drag, such as stability, maneuvrability, and resistance to rough seas, as mentioned in the introduction. They could also come from the assumptions of our model. In particular, a steady motion is considered here, while for rowing boats and sprint canoes, high fluctuations of speed are encountered (about 20% of the mean velocity) and are expected to affect the total drag, notably through added mass.

The data for rowing boats, canoes, and kayaks are found to be in good agreement with the optimal Froude number $\mathrm{Fr}^\star(\Pi)$. For rowing shells, while the aspect ratios α are found quite close to the optimal value, the aspect ratios β lie well above the optimal curve. This indicates that rowing shells could be shorter or have a larger draft. This discrepancy might be related to the need for sufficient spacing between rowers (long shells) and/or for stability (small draft). For sprint canoes and kayaks, the competition rules from the International Canoe Federation [35] impose maximal lengths for the boats [36], which could explain their relatively low aspect ratio α compared to the optimal one. As for their aspect ratio β, contrary to rowing boats, it is found to be in good agreement with the optimal results.

For the monohull sailing boats, the significant difference between real data and the computed optima surely comes from the need for stability (see Appendix C). The stability of a boat mostly depends on the position of its center of gravity (which should be as low as possible) with respect to the position of the metacenter [2,4] (which should in turn be as high as possible). Imposing that the metacenter be above the center of gravity yields a simple criterion for static stability [37]. This is w/d should be larger than a certain value depending on mass distribution and effective density of the hull, which constitutes an additional constraint that could be easily taken into account in the optimization problem. In the simple geometry considered here and assuming a homogeneous body of density ρ_s the latter criterion is $w/d = \beta/\alpha > \psi(\rho_\mathrm{s}/\rho)$, where $\psi(u) \approx 3\sqrt{1/u - 1}$ with $u \in [0,1]$. For real boats, the critical value of w/d is highly affected by the presence of a keel, intended to lower the position of the center of gravity. In short, stability favors wide and shallow ships. This explains why most real data points lie below the optimal curve $\alpha^\star(\Pi)$ in Fig. 5(a) but above the curve $\beta^\star(\Pi)$ in Fig. 5(b). Stability is all the more important for sailing boats where the action of the wind on the sail contributes with a significant destabilizing torque. Interestingly, this matter is overcome for multihull sailing boats, in which both stability and optimal aspect ratios can be achieved by setting the appropriate effective beam, namely the distance between hulls [38]. This allows higher hull aspect ratios, closer to the optimal curves in Fig. 5.

As displayed in Fig. 5(c), we predict a shift in the Froude number for $\Pi \approx 0.2$ which indicates that boats should not operate in the range of Froude numbers $\mathrm{Fr} \in [0.8, 1.7]$. However, when the Froude number is above $\mathrm{Fr} \approx 0.7$, the hulls start riding their own bow wave: They are planing. Their weight is then mostly balanced by hydrodynamic lift rather than static buoyancy [4,7]. As planing is highly dependent on the hull geometry and would require us to consider tilted hulls, we do not expect our model to hold in this regime. Some changes, though, allow us to understand the basic principles. Planing drastically reduces the immersed volume of the hull, which in turn reduces both the wave drag and the profile drag. The effect on the immersed volume can be taken into account by adding the hydrodynamic lift in the momentum balance along the vertical direction (see Ref. [39]).

Our study provides the guidelines of a general method for hull-shape optimization. It does not aim at presenting quantitative results on optimal aspect ratios, in particular due to the simplified geometry we consider and the limitations of Michell's theory for the wave drag estimation [21,27,30]. Our method can be applied in a more quantitative way for each class of boat by considering more realistic hull geometries. Future work should be devoted to applying this method to the category of rowing boats, sprint canoes, and sprint kayaks, as these particular boats mostly require the least drag, with no or little concern for stability and other constraints.

ACKNOWLEDGMENTS

We deeply thank Marc Rabaud for carefully reading the manuscript, and for his wise and thoughtful advice. We also thank Renan Cuzon, Alexandre Darmon, François Gallaire, Tristan Leclercq, Pierre Lecointre, and Elie Raphaël for very fruitful discussions.

APPENDIX A: WAVE DRAG COEFFICIENT

Here we derive the wave drag coefficient and discuss its behavior for parabolic and Gaussian hull shapes. According to Refs. [8,21], the wave drag in Michell's theory is

$$R_{\mathrm{w}}(f) = \frac{4\rho U^2}{\pi \ell^4 \mathrm{Fr}^4} \int_1^{+\infty} \frac{|\mathcal{I}_f(\lambda,\mathrm{Fr})|^2}{\sqrt{\lambda^2-1}}\, d\lambda\ , \tag{A1}$$

where

$$\mathcal{I}_f(\lambda,\mathrm{Fr}) = \frac{\lambda^2}{\mathrm{Fr}^2} \int_{-d}^{0} dz \int_{-\frac{\ell}{2}}^{\frac{\ell}{2}} f(x) e^{\lambda^2 z/(\ell \mathrm{Fr}^2)} e^{i\lambda x/(\ell \mathrm{Fr}^2)}\, dx\ . \tag{A2}$$

Taking $\Omega^{1/3} = (\ell w d)^{1/3}$ as a characteristic length, we define the wave drag coefficient through the equation $R_{\mathrm{w}} = \rho \Omega^{2/3} U^2 C_{\mathrm{w}}$. Then using the dimensionless coordinates $\tilde{x}$, $\tilde{y}$, and $\tilde{z}$ and the dimensionless parameters Fr, α, and β, and integrating over $\tilde{z}$, we obtain the expression of the wave drag coefficient C_{w} given in Eqs. (1) and (2) with $I_{\tilde{f}} = \mathcal{I}_f/(\ell^2 w) = \mathcal{I}_f/(\Omega\beta)$. The wave-drag coefficient compares quite well with previous numerical and experimental works [40,41] as shown in Fig. 6. This plot shows that the wave drag coefficient has the same qualitative evolution with the Froude number for a Gaussian hull and a parabolic hull. The main differences between the two are the presence of humps and hollows at low Froude number for the parabolic profile and a slight

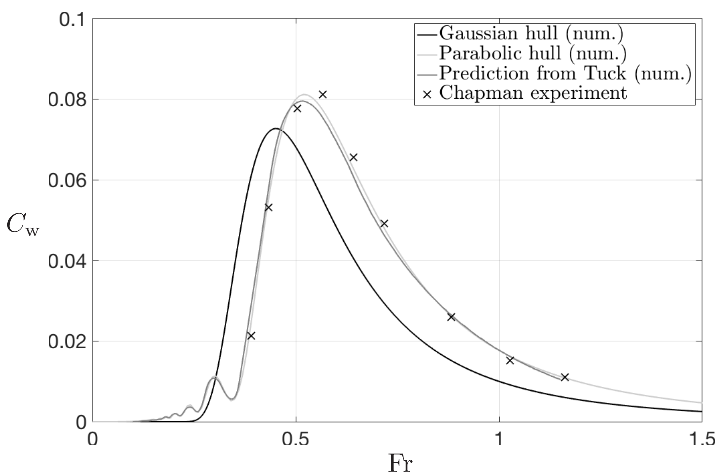

FIG. 6. Wave-drag coefficient C_{w} as function of the Froude number Fr for a Gaussian hull and a parabolic hull for $\alpha = 6.7$ and $\beta = 2.3$. These results are compared to the theoretical curve from Tuck [40] and experimental data points from Chapman (black crosses) [41].

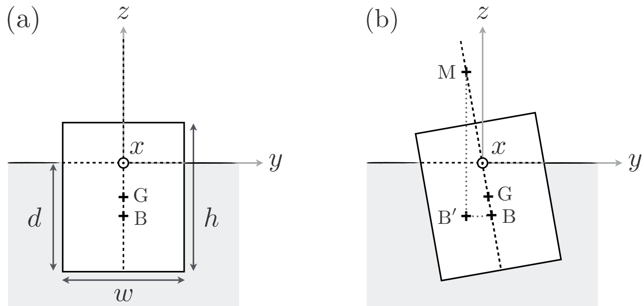

FIG. 7. Cross section of the model hull (see Fig. 3) in (a) vertical position and (b) slightly inclined position.

translation of the peak of wave resistance. For a Gaussian hull, one can approximate analytically the integrals in Eq. (A2) by integrating x over $\mathbb{R}$. One obtains [see Eq. (2)]

$$G_{\text{gauss}}(\text{Fr},\beta) = \frac{\pi}{64} J\left(\frac{1}{32\text{Fr}^4}\right) - \frac{\pi}{32} J\left(\frac{1}{32\text{Fr}^4} + \frac{1}{\beta \text{Fr}^2}\right) + \frac{\pi}{64} J\left(\frac{1}{32\text{Fr}^4} + \frac{2}{\beta \text{Fr}^2}\right), \tag{A3}$$

where

$$J(u) = \int_1^{+\infty} \frac{e^{-u\lambda^2}}{\sqrt{\lambda^2 - 1}}\, d\lambda = \frac{1}{2} e^{-u/2} \mathcal{K}_0(u/2)\,, \tag{A4}$$

with $\mathcal{K}_0(u)$ being the modified Bessel function of the second kind of order zero [42].

APPENDIX B: PROFILE DRAG COEFFICIENT

Here we discuss the derivation of the profile drag coefficient. The profile drag is commonly written as $R_{\text{p}} = (1/2)\rho S C_{\text{d}} U^2$, where S is the wetted surface and C_{d} is the profile drag coefficient of the hull. Here, the wetted surface can be decomposed in two contributions $S = S_{\text{b}} + \mathcal{L} d$, where $S_{\text{b}} = 2w\ell \int_{-1/2}^{1/2} \tilde{f}(\tilde{x})\, d\tilde{x}$ is the surface of the bottom horizontal cross section of the hull and $\mathcal{L} = 2\ell \int_{-1/2}^{1/2} [1 + \tilde{f}'(\tilde{x})^2/\alpha^2]^{1/2}\, d\tilde{x}$ is the perimeter of the hull. This leads to the expression of the coefficient C_{p} given in Eq. (4). As mentioned in the main text, C_{d} depends on the geometry through an empirical relation $C_{\text{d}}(\alpha) = C_{\text{f}}(1 + 2/\alpha + 60/\alpha^4)$ where the skin drag coefficient C_{f} weakly depends on the Reynolds number [7]. In the turbulent regime ($\text{Re} > 5.10^5$), one has the empirical law $C_{\text{f}}(\text{Re}) \simeq 0.075/[\log(\text{Re}) - 2]^2$ [43].

APPENDIX C: STATIC STABILITY CRITERION

Here we explicit the derivation of the stability criterion for the model hull presented in Fig. 3. Consider a homogenous body of density $\rho_s < \rho$ standing at the air-water interface (see Fig. 7). We define the center of gravity G, the center of buoyancy B, and the metacenter M [2,4] as the point of intersection of the line passing through B and G and the vertical line through the new center of buoyancy B′ created when the body is displaced [see Fig. 7(b)]. As mentioned in the main text, the stability criterion reads $\overline{\text{GM}} > 0$, or equivalently $\overline{\text{BM}} > \overline{\text{BG}}$. On the one hand, the so-called metacentric height BM can be computed for small inclination angles through the longitudinal moment of inertia of the body $\mathscr{I} = (8c_{\tilde{f}})w^3\ell/12$ with $c_{\tilde{f}} = \int_{-1/2}^{1/2} [\tilde{f}(\tilde{x})]^3\, d\tilde{x}$ and the immersed volume $\Omega_{\text{i}} = 2a_{\tilde{f}}\Omega$ as

$$\text{BM} = \frac{\mathscr{I}}{\Omega_{\text{i}}} = \frac{c_{\tilde{f}}}{3a_{\tilde{f}}} \frac{w^2}{d}\,. \tag{C1}$$

On the other hand, one has $BG = (h - d)/2$, where h is the total height of the hull. We then use the static equilibrium $\rho_s \Omega_{\rm tot} = \rho \Omega_{\rm i}$, where $\Omega_{\rm tot} = 2a_{\tilde{f}} w \ell h$ is the total volume of the body, to eliminate h. This finally yields the criterion $w/d > \psi(\rho_s/\rho)$ with

$$\psi(u) = \sqrt{\frac{3a_{\tilde{f}}}{2c_{\tilde{f}}}\left(\frac{1}{u} - 1\right)}, \quad u \in [0,1], \tag{C2}$$

where ψ is a decreasing function of u. For neutrally buoyant bodies, $\psi(1) = 0$, all configurations are stable as B and G coincide. While for bodies floating well above the level of water, $\lim_{u\to 0} \psi(u) = +\infty$, wide and shallow hulls are required to ensure stability. In the specific model case of Fig. 3, one has $a_{\tilde{f}} \approx 0.33$, $c_{\tilde{f}} \approx 0.057$, and thus $\psi(u) \approx 3\sqrt{1/u - 1}$. Taking this stability criterion into account in the optimization procedure would reduce the search space and thus constraint the optimum curves to $\beta/\alpha > \psi(\rho_s/\rho)$.

APPENDIX D: EMPIRICAL DATA

Table I presents the characteristics (geometry, mass, typical speed, and estimated propulsive power) of different bodies moving at the water surface, such as different types of ships and some animals.

TABLE I. Characteristics of bodies moving at the water surface. The planing hulls are indicated with (p) in the column Boat name. N.A. stands for *not available*. (*) For all hulls (including planing hulls for which this estimation might be too rough), the draft is estimated using the mass of the boat and the relation $M/\rho \simeq 2a_{\tilde{f}} \ell w d$ (with $a_{\tilde{f}} = 0.33$). The power is estimated through diverse methods depending on the category of the boat. For liners and warships, the propulsive power can easily be found in the specification documents. For rowing boats, canoes, and kayaks, we consider that the power per oarsman is 400 W. For sailing boats and sailboards, we use the sail area of the boat to derive its propulsive power (with a typical wind of 10 m/s). Note that for multihull sailing boats, the indicated dimensions correspond to one of the hulls.

Category	Boat name	Length ℓ (m)	Width w (m)	Draft d (m)	Mass M (kg)	Speed U (m/s)	Power (*) P (kW)
Liner	*Titanic*	269.0	28.00	10.50	52300000	11.70	33833.0
Liner	*Queen Mary 2*	345.0	41.00	8.10	76000000	14.90	115473.0
Liner	*Seawise Giant*	458.0	68.90	31.20	650000000	6.60	37300.0
Liner	*Emma Maersk*	373.0	56.00	15.80	218000000	13.40	88000.0
Liner	*Abeille Bourbon*	80.0	16.50	3.70	3200000	9.95	16000.0
Liner	*France*	300.0	33.70	8.50	57000000	15.80	117680.0
Warship	*Charles de Gaulle*	261.5	31.50	7.80	42500000	13.80	61046.0
Warship	*Yamato*	263.0	36.90	11.40	73000000	13.80	110325.0
Rowing boat	Single scull	8.1	0.28	0.07	104	5.08	0.4
Rowing boat	Double scull	10.0	0.34	0.09	207	5.56	0.8
Rowing boat	Coxless pair	10.0	0.34	0.09	207	5.43	0.8
Rowing boat	Quadruple scull	12.8	0.41	0.12	412	6.02	1.6
Rowing boat	Coxless four	12.7	0.42	0.12	412	5.92	1.6
Rowing boat	Coxed eight	17.7	0.56	0.13	820	6.26	3.2
Canoe	C1	5.2	0.34	0.09	104	4.45	0.4
Canoe	C2	6.5	0.42	0.11	200	4.80	0.8
Canoe	C4	8.9	0.50	0.13	390	5.24	1.6
Kayak	K1	5.2	0.42	0.07	102	4.95	0.4
Kayak	K2	6.5	0.42	0.11	198	5.35	0.8
Kayak	K4	11.0	0.42	0.13	390	6.00	1.6
Sailing boat monohull	*Finn* (p)	4.5	1.51	0.12	240	4.10	4.0

TABLE I. (*Continued.*)

Category	Boat name	Length ℓ (m)	Width w (m)	Draft d (m)	Mass M (kg)	Speed U (m/s)	Power (*) P (kW)
Sailing boat monohull	*505* (p)	5.0	1.88	0.15	300	7.60	18.9
Sailing boat monohull	*Laser* (p)	4.2	1.39	0.10	130	4.10	2.7
Sailing boat monohull	*Dragon*	8.9	1.96	0.50	1000	7.60	16.5
Sailing boat monohull	*Star*	6.9	1.74	0.35	671	7.60	18.5
Sailing boat monohull	*IMOCA 60* (p)	18.0	5.46	0.50	9000	15.30	843.4
Sailing boat monohull	18-ft skiff (p)	8.9	2.00	0.24	420	12.70	85.2
Sailing boat monohull	*49er* (p)	4.9	1.93	0.20	275	7.60	25.9
Sailing boat multihull	*Nacra 450* (p)	4.6	0.25	0.12	330	9.20	20.7
Sailing boat multihull	*Hobie Cat 16* (p)	5.0	0.30	0.12	330	7.60	20.1
Sailing boat multihull	*Macif*	30.0	2.50	0.50	14000	20.40	1218.3
Sailing boat multihull	*Banque populaire V*	40.0	2.50	0.50	14000	23.00	1701.1
Sailing boat multihull	*Groupama 3*	31.5	2.40	0.50	19000	18.50	1407.3
Sailboard	*Mistral One Design* (p)	3.7	0.63	0.05	85	10.20	6.9
Sailboard	*RS:X* (p)	2.9	0.93	0.05	85	11.70	10.2
Motorboat	*Zodiac* (p)	4.7	2.00	0.11	700	17.80	180.0
Animal	Swan	0.5	0.40	0.08	10	0.76	N.A.
Animal	Duck	0.3	0.20	0.13	5	0.66	N.A.
Animal	Human	1.8	0.60	0.13	90	2.00	0.3

[1] K. J. Rawson, *Basic Ship Theory* (Butterworth-Heinemann, Oxford, 2001), Vol. 1.
[2] F. Fossati, *Aero-hydrodynamics and the Performance of Sailing Yachts: The Science behind Sailing Yachts and Their Design* (A&C Black, London, 2009).
[3] L. Larsson, H. C. Raven, and J. R. Paulling, *Ship Resistance and Flow*, Principles of Naval Architecture (Society of Naval Architects and Marine Engineers, Jersey City, NJ, 2010).
[4] R. Eliasson, L. Larsson, and M. Orych, *Principles of Yacht Design* (A&C Black, London, 2014).
[5] J. McArthur, *High Performance Rowing* (Crowood Press, Ramsbury, 1997).
[6] V. Nolte, *Rowing Faster* (Human Kinetics 1, Stanningley, Leeds, 2005).
[7] S. F. Hoerner, *Fluid-Dynamic Drag: Practical Information on Aerodynamic Drag and Hydrodynamic Resistance* (Hoerner Fluid Dynamics, New York, 1965).
[8] J. H. Michell, XI. The wave-resistance of a ship, London, Edinburgh, Dublin Philos. Mag. J. Sci. **45**, 106 (1898).
[9] T. H. Havelock, Wave resistance: Some cases of three-dimensional fluid motion, Proc. Royal Soc. London, Ser. A **95**, 354 (1919).
[10] T. H. Havelock, The theory of wave resistance, Proc. Royal Soc. London, Ser. A **138**, 339 (1932).
[11] F. E. Fish, Influence of hydrodynamic-design and propulsive mode on mammalian swimming energetics, Aust. J. Zool. **42**, 79 (1994).
[12] W. T. Gough, S. C. Farina, and F. E. Fish, Aquatic burst locomotion by hydroplaning and paddling in common eiders (*Somateria mollissima*), J. Exp. Biol. **218**, 1632 (2015).
[13] S. W. McCue and L. K. Forbes, Bow and stern flows with constant vorticity, J. Fluid Mech. **399**, 277 (1999).
[14] S. Percival, D. Hendrix, and F. Noblesse, Hydrodynamic optimization of ship hull forms, Appl. Ocean Res. **23**, 337 (2001).

[15] C.-C. Hsiung, Optimal ship forms for minimum wave resistance, J. Ship Res. **25**, 95 (1981).
[16] B.-J. Zhang, M. Kun, and Z.-S. Ji, The optimization of the hull form with the minimum wave making resistance based on rankine source method, J. Hydrodynam., Ser. B **21**, 277 (2009).
[17] M. Benzaquen, A. Darmon, and E. Raphaël, Wake pattern and wave resistance for anisotropic moving disturbances, Phys. Fluids **26**, 092106 (2014).
[18] C.-C. Hsiung and D. Shenyan, Optimal ship forms for minimum total resistance, J. Ship Res. **28**, 163 (1984).
[19] J. Dambrine, M. Pierre, and G. Rousseaux, A theoretical and numerical determination of optimal ship forms based on Michell's wave resistance, ESAIM **22**, 88 (2016).
[20] E. F. Campana, D. Peri, Y. Tahara, and F. Stern, Shape optimization in ship hydrodynamics using computational fluid dynamics, Comput. Methods Appl. Mech. Eng. **196**, 634 (2006).
[21] E. O. Tuck, The wave resistance formula of JH Michell (1898) and its significance to recent research in ship hydrodynamics, ANZIAM J. **30**, 365 (1989).
[22] T. Inui, *Wave-Making Resistance of Ships* (Society of Naval Architects and Marine Engineers, 1962).
[23] J. V. Wehausen, The wave resistance of ships, Adv. Appl. Mech. **13**, 93 (1973).
[24] In dimensionless coordinates, the hull boundary $y = f(x)$ with $x \in [-\ell/2, \ell/2]$ becomes $\tilde{y} = y/\ell = (w/\ell)\tilde{f}(\tilde{x})$ with $\tilde{x} \in [-1/2, 1/2]$.
[25] E. Raphaël and P.-G. De Gennes, Capillary gravity waves caused by a moving disturbance: Wave resistance, Phys. Rev. E **53**, 3448 (1996).
[26] A. Darmon, M. Benzaquen, and E. Raphaël, Kelvin wake pattern at large Froude numbers, J. Fluid Mech. **738**, R3 (2014).
[27] A. S. Gotman, Study of Michell's integral and influence of viscosity and ship hull form on wave resistance, Ocean. Eng. Int. **6**, 74 (2002).
[28] The immersed volume Ω_i is related to Ω through $\Omega_\mathrm{i} = 2a_{\tilde{f}}\Omega$ [see Eq. (5)].
[29] This empirical expansion is expected to hold for $\alpha \gtrsim 2$ (see Ref. [7]).
[30] F. C. Michelsen, Wave resistance solution of Michell's integral for polynomial ship forms, Ph.D. thesis, The University of Michigan, 1960.
[31] With no constraint on the geometry of the hull, the shape minimizing the wetted surface is a spherical cap.
[32] Note that in order to avoid oscillations due to the sharp edges of the hull, the integral over x in Eq. (2) was actually computed over $\mathbb{R}$ (see Appendix A). We checked that doing so had negligible effect on the results.
[33] R. H. Byrd, J. C. Gilbert, and J. Nocedal, A trust region method based on interior point techniques for nonlinear programming, Math. Program. **89**, 149 (2000).
[34] R. H. Byrd, M. E. Hribar, and J. Nocedal, An interior point algorithm for large-scale nonlinear programming, SIAM J. Optim. **9**, 877 (1999).
[35] International Canoe Federation, Canoe sprint competition rules, www.canoeicf.com/rules.
[36] The maximal lengths for canoes and kayaks are the same for C1 and K1 (5.2 m), C2 and K2 (6.5 m), but not for C4 (9 m) and K4 (11 m) (see also Table I).
[37] Note that for real hull design one should also address dynamic stability [1], but the latter falls beyond the scope of our study.
[38] P. Y. Belly, *250 Réponses aux Questions d'un Marin Curieux* (Le gerfaut, 2004).
[39] Vertical momentum balance writes $Mg \simeq \rho\Omega_\mathrm{i} g + \frac{1}{2}\rho C_L \ell w \sin(2\theta) U^2$, where M is the mass of the boat, Ω_i is the immersed volume, and $\theta(\mathrm{Fr})$ is the Froude-dependent angle of the hull with respect to the horizontal direction of motion [4,7]. This leads to an immersed volume which depends on the Froude number through $\Omega \simeq (M/\rho)/[1 + 0.5 C_L \beta \sin(2\theta)\mathrm{Fr}^2]$. For low Froude number, $\theta(\mathrm{Fr}) \simeq 0$ and the volume is that imposed by static equilibrium, while for larger Fr number $\theta > 0$ and the volume Ω is decreased. Note that foil devices also contribute to decreasing the immersed volume, by increasing the lift.
[40] E. O. Tuck, Wave resistance of thin ships and catamarans, Applied Mathematics Report T8701, 1987.
[41] R. B. Chapman, Hydrodynamic drag of semisubmerged ships, J. Basic Eng. **94**, 879 (1972).
[42] M. Abramowitz and I. A. Stegun, *Handbook of Mathematical Functions: With Formulas, Graphs, and Mathematical Tables* (Courier Corporation, 1964).
[43] J. B. Hadler, Coefficients for international towing tank conference 1957 model-ship correlation line, Technical Report, David Taylor Model Basin, Washington, DC, 1958 (unpublished).